PHYSICAL REVIEW B **68**, 140503(R) (2003)

Real-space imaging of structural transitions in the vortex lattice of V_3Si

C. E. Sosolik,* Joseph A. Stroscio, M. D. Stiles, E. W. Hudson,† S. R. Blankenship, A. P. Fein, and R. J. Celotta
Electron Physics Group, National Institute of Standards and Technology, Gaithersburg, Maryland 20899-8412, USA
(Received 15 August 2003; published 6 October 2003)

The predictions of nonlocal London theory are confirmed by real-space measurements of the hexagonal-to-square transition in the vortex lattice structure of V_3Si. We observe that the lattice transforms from hexagonal to nearly square over the field range of 0–4 T for fields applied along the [001] direction. Above ≈ 0.75 T, we find that the lattice orientation is strongly linked to the symmetry of the underlying V_3Si crystal and has a (100) symmetry plane. Near the rhombus-to-square transition at 4 T, we observe anisotropic long-range translational order, consistent with predictions of the elasticity of the lattice near this transition.

DOI: 10.1103/PhysRevB.68.140503 PACS number(s): 74.25.Qt, 74.70.Ad, 68.37.Ef

In type-II superconductors, the expulsion of the magnetic field from the superconductor, called the Meissner effect, is not complete for fields above the lower critical field H_{C1}. In this regime, magnetic fields penetrate into the bulk by forming vortices with a core in which the superconductivity is suppressed and a circulating current surrounds the core. The magnetic flux in each vortex is quantized in units of the flux quantum ($\Phi_0 = h/2e$). Superconductors are characterized by two lengths, the coherence length ξ and the penetration length λ, which is the length scale over which the magnetic field can penetrate the superconducting state. In type-II superconductors the ratio of these lengths, $\kappa = \lambda/\xi$, is greater than $1/\sqrt{2}$. When κ is large, the vortex state exists over a large field range. The vortices interact with each other through the circulating currents around each vortex and form a lattice in equilibrium.[1,2] The currents reflect the symmetry of the electronic states and give rise to a complex evolution of vortex lattice structures with applied field.[3]

Recent work on vortex-vortex interactions in high-κ superconductors, such as the nonmagnetic borocarbide and A15 materials, has focused on understanding the relationship between the vortex lattice symmetry and the underlying symmetry of the superconductor,[4–6] in particular, the progression from simple hexagonal packing to more square geometries with increased field. Kogan *et al.* have made calculations that directly relate these changes in lattice symmetry to the effects of nonlocality within the framework of the London theory.[5] The *nonlocality* arises from the finite size of the Cooper pairs ξ_0 and accounts for the fact that the current density at any position **r** is determined by the vector potential within a region of radius $\approx \xi_0$ about that position.[1,2] This connection between the current density and the vector potential implies that the symmetry of the Fermi surface will be reflected in the vortex-vortex interactions and ultimately in the structure of the vortex lattice.

The vortex lattice in V_3Si, a high-κ material ($\kappa \approx 20$), was one of the first systems where the London theory with nonlocal contributions was applied.[4] For an applied field parallel to the [001] direction, the nonlocal London theory predicts two regimes defined by the fields H_1 and H_2. For applied fields below H_1, a vortex lattice with a rhombic unit cell is predicted with a mirror plane along the [110] direction. In this regime the apex angle of the rhombus decreases from 60° (a hexagonal lattice) as the field increases from H_{C1}. For applied fields above H_1, a 45° reorientation of the unit cell is predicted with a mirror symmetry plane along the [100] direction and an apex angle greater than 60° that increases with increasing field. Eventually, the rhombic unit cell transforms into a square unit cell at H_2.

Yethiraj *et al.* made precise small-angle neutron-scattering (SANS) measurements of vortex lattices for fields of up to 1.5 T applied along the [001] direction in V_3Si.[6] They observed a square unit cell for fields above 1 T and a distorted rhombic unit cell with (110) symmetry at lower fields that exhibited the behavior predicted for V_3Si below H_1. The predicted reorientation transition at $H_1 = 0.4$ T into a lattice with (100) symmetry was not seen, however, and this stimulated our search to measure both a vortex lattice in V_3Si with (100) symmetry and the associated reorientation between the (110) symmetric and the (100) symmetric unit cells. A reorientation transition analogous to that predicted for V_3Si at H_1 has been reported in the borocarbide superconductors $LuNi_2B_2C$ (Ref. 7) and YNi_2B_2C (Refs. 8,9).

In this paper, we test nonlocal London theory by comparing its predictions to the results of real-space measurements of structural transitions in the vortex lattice of V_3Si. Fundamentally, our results demonstrate that large-scale imaging of a superconductor in ultra-high vacuum (UHV) with a scanning tunneling microscope (STM) is a viable technique for obtaining real-space measurements of the high-density vortex lattices that occur in high magnetic fields. Our images of the vortex lattice in V_3Si are large enough to compute reciprocal space properties that can be directly compared with neutron-scattering experiments. We can also observe the evolution of the lattice from hexagonal to square at ≈ 4 T for a field applied along the [001] direction. Further, we find that the vortex lattice has mirror plane symmetry around the (100) crystal plane for fields above ≈ 0.75 T. Finally, we observe strong anisotropy in the long-range translational order as the lattice becomes square. These results complement previous SANS data for V_3Si (Ref. 6) and are in excellent agreement with the theory of Kogan *et al.*[4,10] based on the London theory with nonlocal corrections.

Measurements of the vortex lattice were performed in UHV in a low temperature STM system on a single crystal V_3Si (001) sample. The sample was 2.0-mm thick and had a

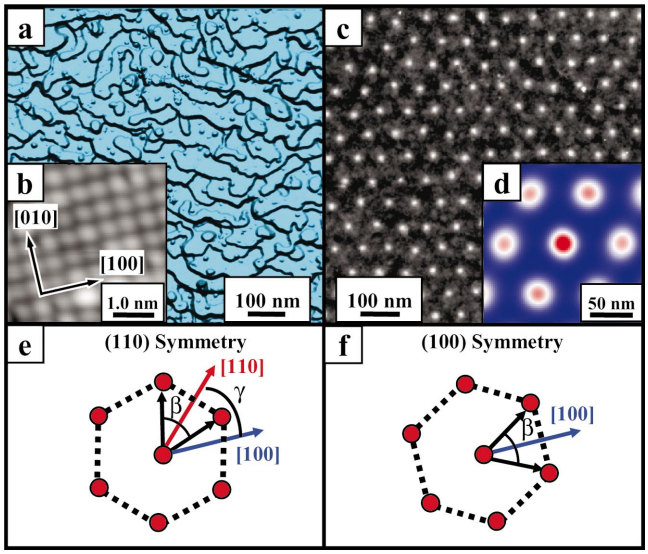

FIG. 1. (Color) (a) STM topographic image, 818×818 nm^2, of the $V_3Si(001)$ surface obtained at 2.3 K shown in a side-lighted view. The tunneling current and sample bias are 0.25 nA and -10 mV, respectively. (b) Atomic resolution STM topograph of $V_3Si(001)$ showing the Si sublattice and the orientation of the crystallographic axes. (c) Vortex lattice image at 0.25 T applied field seen in the Fermi-level normalized differential conductance image obtained simultaneously with the topographic image in (a). (d) Auto-correlation image of the vortex lattice in (c) showing a unit cell with (110) mirror plane symmetry. (e-f) Schematics of vortex lattice unit cells with (110) and (100) mirror plane symmetries, respectively.

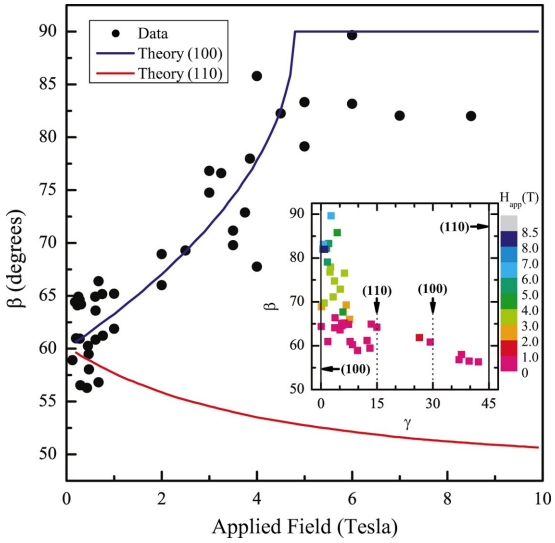

FIG. 3. (Color) (symbols) Measured apex angle [see schematic in Figs. 1(e) and 1(f)] of the vortex lattice unit cell as a function of applied magnetic field. Below 1 T, the applied field was obtained from the vortex density in the lattice images. The statistical error associated with the measured values is on the order of the displayed symbol size. Repeated cycling of the applied field gives rise to the scatter in the observed β values, presumably due to hysteresis effects. (solid lines) Calculated apex angle using nonlocal London theory. (Inset) The measured apex angle as a function of the orientation of the unit cell. The symmetry planes indicated at 15 and 30 degrees result from the existence of multiple mirror planes for hexagonal lattices. The color bar denotes the applied magnetic field for these data.

polished (001) face that measured 2.0×7.0 mm^2. SQUID magnetometry was used to characterize the crystal, and a transition temperature of $T_C\approx16.8$ K was obtained. From the measured slope of $dH_{C2}/dT=-1.9$ T/K we extract an estimate of $H_{C2}(0)\approx22$ T. Electrical resistivity measurements on the sample yield a residual resistance ratio $=29$. The $V_3Si(001)$ crystal surface was cleaned by repeated neon ion bombardment and annealing to 750 °C. Directly after cleaning, the crystal was transferred in UHV into the STM, along with a field evaporation cleaned Ir probe tip, and cooled to 2.3 K in zero field. A typical large-scale topography mea-

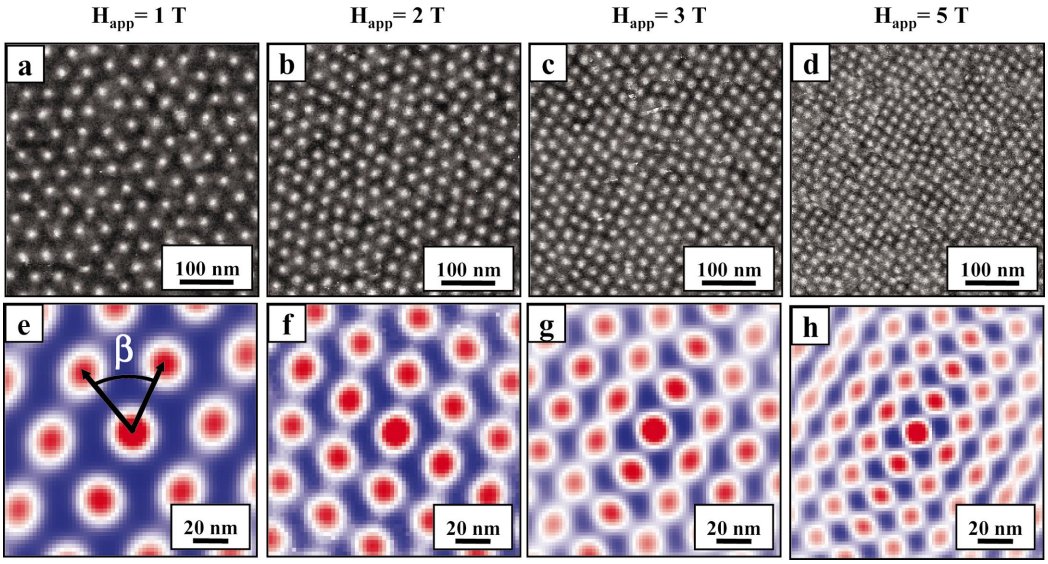

FIG. 2. (Color) (a)–(d) Vortex lattice images from the Fermi-level differential conductance maps and (e)–(h) corresponding autocorrelation images, as a function of applied magnetic field.

surement of the crystal surface [Fig. 1(a)] shows single atom high steps with an average terrace width of ≈ 50 nm. Atomic resolution topography, such as the example shown in Fig. 1(b), reveals the underlying Si sublattice, which has a unit cell spacing of 4.73 Å. Figure 1(b) reveals the horizontal scan direction, used in all of our measurements, to be rotated 14° relative to the [100] crystal axis.

To map the vortex lattice, large-scale spatial maps of the differential conductance were made as a function of the magnetic field applied parallel to the [001] crystal axis. The normalized differential conductance is a measure of the quasiparticle density of states in the superconductor at a position $\mathbf{r}$ and is defined as $N(\mathbf{r},E)=[dI/dV(\mathbf{r},E)/dI/dV(\mathbf{r},E_S)]$, where E_S is the setpoint energy for the measurement (typically -10 meV).[11] The vortex lattice can be imaged by examining a spatial map of the normalized differential conductance at the Fermi level $N(\mathbf{r},E_F)$ such as that shown in Fig. 1(c). All the vortex lattice measurements were performed after zero-field cooling the sample below T_C. The maps were obtained at several distinct spatial positions over an area of ≈ 5 μm near the sample center, and the applied field was repeatedly ramped to values between 0 and 8.5 T with the crystal held at 2.3 K.

Images of the vortex lattice at each applied field were analyzed by taking an autocorrelation of the measured differential conductance maps. The nearest-neighbor spots in the autocorrelation image represent an average unit cell for the vortex lattice in a given map [see Fig. 1(d)]. We characterize the vortex lattice in each autocorrelation image in terms of a rhombic unit cell which has an apex angle β and a diagonal that lies at an angle γ with respect to the [100] direction [Fig. 1(e)]. The angle γ defines a generalized symmetry plane for the vortex lattice and allows for values that are not along the crystal symmetry axes. Examples of a hexagonal lattice with (110) ($\gamma=45°$) or (100) ($\gamma=0°$) symmetry planes are shown in the schematics of Figs. 1(e) and 1(f). These are the two symmetry planes predicted for the vortex lattice in V_3Si.[4] One should note that degenerate orientations for the hexagonal lattice that correspond to a rotation of each hexagon in Figs. 1(e) and 1(f) by 90° also exist. For example, the autocorrelation shown in Fig. 1(d) has a (110) symmetry plane and is rotated 90° from the schematic of Fig. 1(e). In the results presented here, we fold all measured γ values into the range between 0° and 45°, or (100) and (110) symmetry planes, respectively. Using this convention, additional (110) and (100) symmetry planes occur for a hexagonal lattice at 15° and 30°, respectively.

A set of differential conductance images and autocorrelations for four applied magnetic fields between 1 and 5 T is shown in Fig. 2. The differential conductance images clearly show the decrease in nearest-neighbor distance as the applied field is increased, and the autocorrelation of each image shows that the lattice changes from nearly hexagonal to nearly square as the vortices move closer together. This change in lattice structure is summarized in Fig. 3, where the results of many measurements at applied fields up to 8.5 T are shown. At all applied fields, the vortex unit cell is rhombic and the lattice structure only approaches hexagonal ($\beta=60°$) in the limit of zero field. As the field is increased up to 4 T the lattice structure shifts toward square, and the value of the apex angle saturates at $\beta\approx 83°-90°$ for higher applied fields. This change in lattice structure is close to the hexagonal-to-square transition field of 3 T predicted by Kogan *et al.*[4]

In the inset to Fig. 3, the apex angle obtained for each vortex lattice is shown as a function of both the symmetry plane and the magnetic field. At all applied fields above 0.75 T, we see evidence for (100) as a symmetry plane for the vortex lattice. Below 0.75 T, where the lattice is nearly hexagonal, we observe (100), (110), and randomly oriented symmetry planes. This result is consistent with the work of Kogan *et al.*, who predicted a 45° reorientation transition from (100) to (110) symmetry planes as the field was decreased below $H_1=0.4$ T.[4] The fact that orientations other than the ground-state (110) symmetry plane are observed below 0.75 T is consistent with the prediction of the nonlocal theory of a very weak orientation dependence of the energy for fields below H_1. The fact that our results differ from those presented in Ref. 6, where only the (110) symmetry plane was observed for the hexagonal lattice, could be due to differences in vortex lattice preparation (field cooling in Ref. 6 vs zero-field cooling in the present measurements) or measurement technique (SANS vs scanning tunneling microscopy). Of particular interest is the fact that the SANS results clearly mapped out the predicted low-field ($H<H_1$) ground state with the lattice oriented with (110) symmetry, whereas the measurements presented here predominately shows the high field ($H>H_1$) or (100) symmetry state.

We have carried out calculations of the nonlocal corrections to the London equations using the model of Kogan *et al.*[4,5] to calculate the energetically favorable orientations of the vortex lattice as a function of applied magnetic field. This approach is based on a minimization of the Gibbs free energy for vortices formed with $\mathbf{H}\parallel[001]$ and requires Fermi-surface parameters as input. The theory[4] also requires one sample-dependent parameter C that is not readily accessible from experiment. Here we use Fermi-surface parameters for V_3Si from Ref. 4 and adjust the value of C to fit our measured results for the apex angle as a function of field. Vortex lattices for the two symmetry planes, (110) and (100), are considered separately, and a value of the apex angle that minimizes the free energy for applied fields up to 8.5 T is obtained. The results of these calculations are shown in Fig. 3, where the (110) and the (100) symmetry planes are shown as red and blue lines, respectively. As seen in Fig. 3, we observe very good agreement for the hexagonal to square transition, using a value of C equal to one half that used by Kogan *et al.* to fit the SANS data. This difference in C values could arise from the dependence of C on sample-dependent parameters, such as impurity scattering time-scales and superconducting properties, or on the different method of vortex lattice preparation used for the samples.

Our calculation shows that the (110) symmetry plane is the lower-energy configuration below $H_1\approx 1.1$ T. However, we find that the calculated difference in energy between lattices with the (110) and the (100) symmetry planes is very small, which is consistent with a lack of strong orientational order as found in the data shown in the inset of Fig. 3.

The effects of nonlocal electrodynamics are also observed in the long-range translational order (LRO) of the vortex lattice with increasing applied field. At applied fields below ≈ 2 T, the vortex lattices in Fig. 2 are seen to have very weak disorder with relatively large dislocation-free areas in the ≈ 1 μm regions that were scanned. An interesting change occurs in the LRO, however, as the field is increased. As the lattice structure shifts from hexagonal to square, a significant degree of anisotropy develops in the LRO. This anisotropy, which is similar to that observed in $LuNi_2B_2C$,[7] is evident in the differential conductance image and the corresponding Fourier transform (FFT) of Figs. 4(a) and 4(b), which were obtained at 3.25 T. In the differential conductance image, well-ordered parallel rows of vortices are present across the scanned region along the $[\bar{1}10]$ direction, whereas the alignment in the [110] direction is wavy. This anisotropy in LRO is easily seen in the FFT image [Fig. 4(b)], as the reciprocal lattice maxima corresponding to order along the $[\bar{1}10]$ rows are significantly sharper than the corresponding [110] maxima. This anisotropic LRO can be attributed to the anisotropic elasticity of the vortex lattice calculated within nonlocal London theory. Specifically, it has been predicted that the shear modulus of the square vortex lattice is much smaller along the square sides ($[\bar{1}10]$ or [110]) than along the diagonals ([100] or [010]).[10] Therefore, the lattice is more likely to shear along either the $[\bar{1}10]$ or the [110] direction, leading to misaligned vortex rows along the direction perpendicular to this shear. Shearing along one of these directions suppresses shear along the other. The anisotropy is most pronounced around the hexagonal-to-square transition, which is also predicted within nonlocal London theory.

In summary, we have observed the evolution of the vortex lattices of V_3Si as a function of magnetic field with real-space measurements by scanning tunneling spectroscopy.

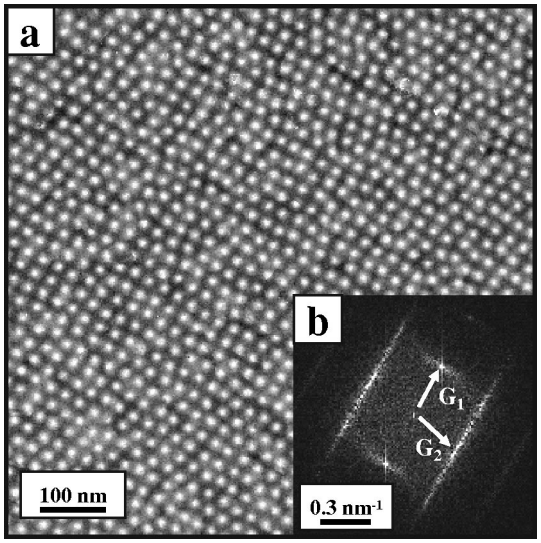

FIG. 4. (a) Vortex lattice image obtained near the rhombic-to-square transition region at an applied field of 3.25 T. (b) Corresponding Fourier transform of (a) showing the anisotropy in the long-range order along the directions corresponding to the reciprocal lattice vectors, G_1 and G_2.

The hexagonal-to-square transition is observed over the field range of 0–4 T for fields applied along the [001] direction, and the orientation of the lattice is strongly tied to the underlying crystal symmetry for fields above ≈ 0.75 T. Close to the transition to a square lattice, a large anisotropy is observed in the long-range translational order.

The authors thank David Tanner for providing the V_3Si crystal used in these measurements and M.C. Boyer, Kittiwit Matan, and Young Lee for the SQUID magnetometry and resistivity measurements. This work was supported in part by the Office of Naval Research.

*Present address: Department of Physics and Astronomy, Clemson University, Clemson, SC 29634.

†Present address: Department of Physics, Massachusetts Institute of Technology, Cambridge, MA 02139.

[1] M. Tinkham, *Introduction to Superconductivity* (McGraw-Hill, New York, 1996).

[2] C.P. Poole, H.A. Farach, and R.J. Creswick, *Superconductivity* (Academic, California, 1995).

[3] N. Nakai, P. Miranovic, M. Ichioka, and K. Machida, Phys. Rev. Lett. **89**, 237004 (2002).

[4] V.G. Kogan, P. Miranovic, Lj. Dobrosavljevic-Grujic, W.E. Pickett, and D.K. Christen, Phys. Rev. Lett. **79**, 741 (1997).

[5] V.G. Kogan, M. Bullock, B. Harmon, P. Miranovic, Lj. Dobrosavljevic-Grujic, P.L. Gammel, and D.J. Bishop, Phys. Rev. B **55**, R8693 (1997).

[6] M. Yethiraj, D.K. Christen, D. McK. Paul, P. Miranovic, and J.R. Thompson, Phys. Rev. Lett. **82**, 5112 (1999).

[7] L.Ya. Vinnikov, T.L. Barkov, P.C. Canfield, S.L. Bud'ko, J.E. Ostenson, F.D. Laabs, and V.G. Kogan, Phys. Rev. B **64**, 220508(R) (2001).

[8] D.M. Paul, C.V. Tomy, C.M. Aegerter, R. Cubitt, S.H. Lloyd, E.M. Forgan, S.L. Lee, and M. Yethiraj, Phys. Rev. Lett. **80**, 1517 (1998).

[9] S.J. Levett, C.D. Dewhurst, and D.M. Paul, Phys. Rev. B **66**, 014515 (2002).

[10] P. Miranovic and V.G. Kogan, Phys. Rev. Lett. **87**, 137002 (2001).

[11] H.F. Hess, R.B. Robinson, R.C. Dynes, J.M. Valles, and J.V. Waszczak, Phys. Rev. Lett. **62**, 214 (1989); M. Ichioka, N. Hayashi, and K. Machida, Phys. Rev. B **55**, 6565 (1997).